^1H and ^{15}N Resonance Assignments of Oxidized Flavodoxin from *Anacystis nidulans* with 3D NMR†

Robert T. Clubb,‡,§ V. Thanabal,‡ C. Osborne,§ and Gerhard Wagner*,‡

Biophysics Research Division, Department of Biological Chemistry, University of Michigan, 2200 Bonisteel Boulevard, Ann Arbor, Michigan 48109, and Department of Biological Chemistry and Molecular Pharmacology, Harvard Medical School, 240 Longwood Avenue, Boston, Massachusetts 02115

Received March 28, 1991; Revised Manuscript Received May 22, 1991

ABSTRACT: Proton and nitrogen-15 sequence-specific nuclear magnetic resonance assignments have been determined for recombinant oxidized flavodoxin from *Anacystis nidulans* (169 residues, M_r 19048). Assignments were obtained by using ^{15}N-^1H heteronuclear three-dimensional (3D) NMR spectroscopy on a uniformly nitrogen-15 enriched sample of the protein, pH 6.6, at 30 °C. For 165 residues, the backbone and a large fraction of the side-chain proton resonances have been assigned. Medium- and long-range NOE's have been used to characterize the secondary structure. In solution, flavodoxin consists of a five-stranded parallel β sheet involving residues 3–9, 31–37, 49–56, 81–89, 114–117, and 141–144. Medium-range NOE's indicate the presence of several helices. Several ^{15}N and ^1H resonances of the flavin mononucleotide (FMN) prosthetic group have been assigned. The FMN-binding site has been investigated by using polypeptide–FMN NOE's.

Flavodoxin from *Anacystis nidulans* is a member of a group of low molecular weight flavoproteins (14000–19000 daltons) that serve as electron transferases in a number of biological reactions (Mayhew & Ludwig, 1975). The electron transfer function of flavodoxins is carried out by a noncovalently attached FMN[1] group. In vitro, the protein-bound flavin occurs in three distinct redox states: oxidized (quinone), a one electron reduced (semiquinone), and a two electron reduced (hydroquinone) form. In vivo, however, flavodoxins shuttle between the semiquinone and hydroquinone states. Flavodoxins are often produced under iron deficient conditions as a replacement for ferredoxin but in some cases they are produced constitutively (Tollin & Edmonson, 1980).

A. nidulans flavodoxin contains 169 amino acids and has molecular weight over 19000 daltons. It is a member of the "long-chain" class of flavodoxins that include among others flavodoxins isolated from *Azotobacter vinelandii*, *Klebsiella pneumoniae*, *Chondrus crispus*, and *Anabaena* 7120. The redox properties of the semiquinone–hydroquinone (E_1) and oxidized–semiquinone (E_2) transitions of FMN are strongly altered upon association with the apoprotein. In *A. nidulans* the E_1 and E_2 redox potentials are −221 and −447 mV (Entsch & Smillie, 1972), while the potentials of free flavin are −172 and −238 mV, respectively (Draper & Ingraham, 1968).

Flavodoxins have been the focus of both crystallographic and NMR studies. Crystal structures have been obtained for several variants (Watenpaugh et al., 1973; Burnett et al., 1974; Smith et al., 1977; Fukuyama et al., 1990; Luschinsky et al., 1991; Watt et al., 1991) including a structure of oxidized flavodoxin from *A. nidulans* at 1.7-Å resolution (Smith et al., 1983; Ludwig et al., 1984). Recently, spectra of oxidized and reduced flavodoxin from *Megasphaera elsdenii* have been assigned (Mierlo et al., 1990a,c), and the solution structure of the reduced form has been calculated. This was achieved by using restrained molecular dynamics calculations starting with the crystal structure from *Clostridum beijerinckii* (Smith et al., 1977) as a model (Mierlo et al., 1990b). These studies indicate that members of the flavodoxin family share a similar global fold. The structural topology of the FMN-binding site, however, has been shown to vary among these flavodoxins thus far studied. This structural observation is consistent with the wide variation in redox potentials exhibited by members of the flavodoxin class.

We have undertaken NMR studies of flavodoxin from *A. nidulans* to gain an understanding of polypeptide–FMN interactions that alter the redox potential of the bound flavin. Elucidation of these interactions requires highly resolved solution structures of both quinone and hydroquinone forms of the protein; the semiquinone form is paramagnetic. Assigning a sufficient number of constraints to determine a structure of a protein of flavodoxin's size would have been impossible in the recent past because of inherent resonance overlap. However, recent methodological advances have made the determination of the solution structure of flavodoxin a tractable problem. Multinuclear editing experiments are capable of resolving resonance overlap, in particular, three-dimensional heteronuclear NMR experiments have proved quite useful (Zuiderwig & Fesik, 1988; Marion et al., 1988). We have

† This research was supported by NIH Grant GM 38608. C.O. was supported by NIH Grant GM 16429.

* Address correspondence to this author.
‡ University of Michigan.
§ Harvard Medical School.

[1] Abbreviations: DQF-COSY, two-dimensional double-quantum filtered correlation spectroscopy; 2Q-COSY, two-dimensional double-quantum spectroscopy; EDTA, ethylenediaminetetraacetic acid; FMN, flavin mononucleotide; HMBC, two-dimensional heteronuclear ^1H-detected multiple bond correlation; HMQC, two-dimensional heteronuclear multiple-quantum coherence; INEPT, insensitive nuclei enhancement by polarization transfer; NMR, nuclear magnetic resonance; NOE, nuclear Overhauser enhancement; NOESY, two-dimensional nuclear Overhauser enhancement spectroscopy; PMSF, phenylmethanesulfonyl fluoride; ROE, rotating frame nuclear Overhauser enhancement; ROM, read only memory; SCUBA, stimulated cross peaks under bleached alphas; SDS-PAGE, sodium dodecyl sulfate–polyacrylamide gel electrophoresis; TOCSY, two-dimensional total correlation spectroscopy; TLCK, Nα-*p*-tosyl-L-lysine chloromethyl ketone; Tris, tris(hydroxymethyl)aminomethane.

0006-2960/91/0430-7718$02.50/0

therefore uniformly enriched flavodoxin with nitrogen-15 in order to resolve overlapped resonances in the homonuclear spectra in a third dimension.

We report here the sequential resonance assignment of ^1H and ^{15}N nuclei in oxidized flavodoxin from *A. nidulans*. Characteristic NOE connectivities and hydrogen exchange patterns indicate that flavodoxin adopts in solution a secondary structure similar to the crystal structure. The core of flavodoxin consists of a five-stranded parallel β sheet formed by residues 3–9, 31–37, 49–56, 81–89, 114–117, and 141–144. Medium range NOE's indicate that residues 12–21, 40–46, 103–114, 145–148, and 152–169 form helices in solution. Resonance assignments are a prelude to a solution structure determination based solely on NMR constraints. Assignments will allow measurement of amide proton exchange rates and ^{15}N–^1H relaxation parameters yielding dynamical information. A molecular level understanding of the redox potential control exhibited by the apoprotein over the flavin prosthetic group requires both NMR and X-ray crystallography. Oxidation state dependent structural changes in both wild-type and active-site mutants of flavodoxin are therefore being approached in a collaborative manner.

Materials and Methods

Protein Expression and Purification. The nucleotide sequence coding for flavodoxin from *A. nidulans* (Laudenbach et al., 1988) resided in a pKK233-2 vector. Transfection of this plasmid into *Escherichia coli* strain W1485 resulted in expression of flavodoxin as judged by UV–visible absorbance of the purified protein. Cells were grown on rich Hershey medium (Hershey, 1955) with glucose as the carbon source. Cultures were shaken at 37 °C for 10 h before harvesting by centrifugation at 6000*g*, 4 °C. Typically harvested cells were dark gray, indicative of flavodoxin in the semiquinone state.

The protocol used for purification of flavodoxin was based on that of Smillie et al. (1965) and Mayhew and Massey (1969). Cell pellets from 1 L of culture were resuspended in 50 mL of buffer. The buffer, hereafter referred to as TE buffer, consisted of 5 mM Tris and 0.3 mM EDTA adjusted to a pH of 7.8. Aprotinin, TLCK, and PMSF were added to the suspension to prevent proteolytic degradation. The cells were then lysed by repeated sonication on ice. Centrifugation of the lysate at 10000*g*, at 4 °C for 90 min, resulted in a dark gray supernatant rich in flavodoxin. The cell lysate was then added along with an equal volume of H_2O to 50 g of preequilibrated DEAE material and stirred on ice for 30 min. The slurry was vacuum filtered with an aspirator. The filter cake was dissolved in 100 mL of TE buffer, 200 mM in KCl. This mixture was stirred on ice for 30 min and filtered. The 200 mM KCl TE buffer wash was then repeated a second time. Flavodoxin was removed from the DEAE by addition of 100 mL of TE buffer, 600 mM in KCl. This mixture was stirred on ice for 30 min. The filtrate was diluted with TE buffer to obtain a final KCl concentration of 100 mM. This mixture, typically 700–900 mL, was loaded onto a DEAE anion-exchange column. Flavodoxin was eluted with TE buffer by using a linear gradient of 100–600 mM KCl with a flow rate of 0.5 mL/min. Flavodoxin eluted at approximately 275 mM KCl.

The pooled fractions were then concentrated on a 4 × 1 cm DEAE column. Typically, from 6 L of culture, flavodoxin eluted from this column into a final volume of 1 mL. Electrophoresis using a nondenaturing gel (3 mm thick) was employed for the final separation. Flavodoxin was layered onto the preparative gel and run at constant current with 60 mA. The yellow band corresponding to flavodoxin was electroeluted with a constant voltage of 200 V. The final product was judged to be pure by both SDS–PAGE and UV–Vis absorbance.

Uniform Enrichment. Nitrogen-15 was uniformly incorporated into flavodoxin by modifying the media used in bacterial growth. The media was identical with that described above with two exceptions. (1) Case amino acids were replaced with a uniformly ^{15}N-enriched polypeptide mixture derived from an algal lysate (Martek Corp.). Preliminary growth studies indicated that 2 g of lysate per liter of culture was sufficient for adequate bacterial growth. (2) 1.2 g of $^{15}NH_4Cl$ per liter of culture was substituted for $^{14}NH_4Cl$.

NMR Sample Preparation. NMR samples were typically 3–4 mM flavodoxin in 0.4 mL of 20 mM phosphate buffer. The pH (uncorrected for isotope effects) was adjusted to 6.6. Spectra collected with H_2O as the solvent contained 5% (v/v) ^2H_2O to establish a lock signal. When ^2H_2O was used as the solvent, the protein was lyophilized and redissolved in ^2H_2O several times.

2D NMR Spectroscopy. All spectra were recorded at 30 °C on a General Electric GN-500 (11.7 T) spectrometer or its corresponding upgrade, the Ω-500. NMR data were processed on SUN workstations using FTNMR (Hare Research, Inc.). ^1H chemical shifts were referenced to internal TSP at pH 6.6, 30 °C. ^{15}N chemical shifts were referenced to external $^{15}NH_4Cl$ (2.9 M) in 1 M HCl at 20 °C, 24.93 ppm relative to NH_3 (Levy & Lichter, 1979).

Experiments were collected in the quadrature mode. A sweep width of 8333.33 Hz was used in both proton dimensions. All experiments were performed in H_2O unless otherwise indicated. Low-power continuous wave saturation was employed during the relaxation delay to suppress the H_2O signal. The relaxation delay was 1.3 s. The SCUBA technique (Brown et al., 1988) was utilized in all experiments to recover saturated proton resonances under the water line. All experiments employed time-proportional phase incrementation (TPPI) for sign discrimination along ω_1 (Marion & Wüthrich, 1983). All data sets were acquired with 4096 points along t_2. Prior to Fourier transformation, the data were multiplied with appropriately matched sine bell window functions in both t_1 and t_2.

The NOESY (Jeener et al., 1979; Kumar et al., 1980) spectrum shown was acquired with a mixing time of 100 ms with 96 transients per t_1 value. A total of 750 t_1's were collected. The 2D total correlation (TOCSY) spectrum (Braunschweiler & Ernst, 1983) was recorded with a MLEV-17 (Bax & Davis, 1985) mixing sequence. Delays were introduced to eliminate cross peaks due to ROE magnetization transfer during the spin lock (clean-TOCSY) as described by Griesinger et al. (1986). An optimum clean-TOCSY delay was determined by comparison of several 2D spectra with varying delays and was found to be 35 μs in duration. The TOCSY spectrum was recorded with mixing times of 55, 75, and 95 ms, which were coadded to a single file. A total of 256 t_1 values were collected per mixing time with 32 scans acquired for each t_1. DQF-COSY (Piantini et al., 1984; Shaka & Freeman, 1983; Rance et al., 1984) spectra were recorded in both H_2O and ^2H_2O. 500 and 700 t_1's were acquired for the H_2O and ^2H_2O experiments, respectively. Two quantum correlation spectra (Bax et al., 1981; Wagner & Zuiderweg, 1983) were acquired in H_2O. A total of 128 transients were acquired per t_1 with a 1000 t_1's recorded. Two-dimensional ^1H-detected heteronuclear chemical shift correlation spectra were obtained by using INEPT type transfers (Morris & Freeman, 1979; Bodenhausen & Ruben, 1980). The ^{15}N sweep width was 5000 Hz. A total of 512

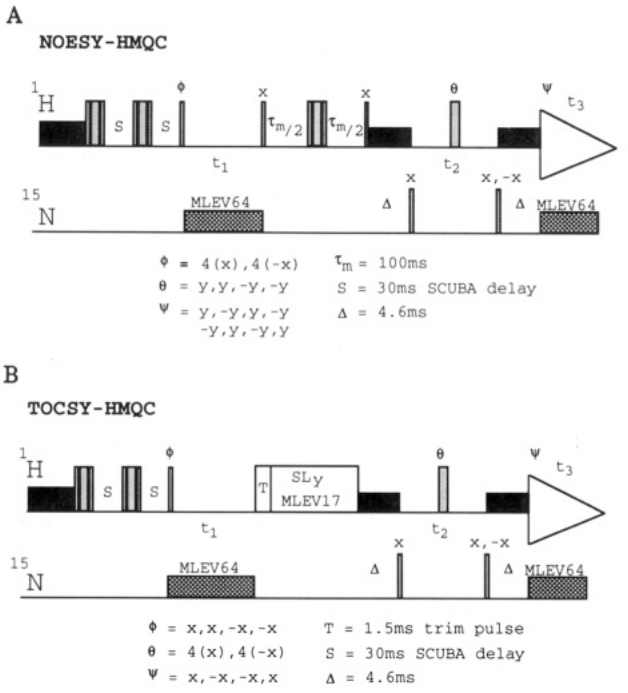

FIGURE 1: (A) 3D HMQC-NOESY pulse sequence. Wide and narrow vertical bars represent 180° and 90° pulses, respectively. The phase cycling used is listed below the sequence. Both panels A and B are similar to pulse sequences described by Zuiderwig and Fesik (1989) and Marion et al. (1989). Low-power H_2O saturation was used during the relaxation and dephasing/rephasing delays (rectangular boxes in the proton channel). Composite ^1H 180° pulses separated by a 30-ms delay were used to recover saturated $C^\alpha H$ proton resonances (SCUBA). A composite ^1H 180° pulse was used in the center of the mixing time (τ_m). (B) 3D HMQC-TOCSY pulse sequence. The figure is analogous to panel A. The ^1H spin lock was preceded by a 1.5-ms trim pulse. MLEV17 was used in the mixing period. Mixing times of 37, 56, 74, and 93 ms were coadded.

t_1's were acquired with 32 scans per t_1. The HMBC spectrum was recorded as described by Bax and Summers (1986). The ω_2-edited NOESY experiment (Otting et al., 1986; Bax & Weiss, 1987) was acquired with a mixing time of 100 ms.

3D NMR Spectroscopy. 3D NOESY-HMQC and TOCSY-HMQC spectra were acquired in a similar manner as described by Zuiderwig and Fesik (1989) and Marion et al. (1989). However, in both 3D experiments, continuous wave low-power saturation was used during the relaxation delay to eliminate the H_2O signal. The 3D NOESY-HMQC and 3D TOCSY-HMQC pulse sequences are shown in Figure 1. SCUBA delays were employed to recover saturated α proton resonances. The relaxation delay was 1.3 s. Protons were decoupled from nitrogen-15 during acquisition by a ROM-based MLEV-64 sequence (Levitt & Freeman, 1981). Sweep widths of 7143, 1600, and 8333 Hz were used in the ω_1, ω_2, and ω_3 dimensions, respectively. TPPI was used in the t_1 and t_2 dimensions to achieve sign discrimination of the frequencies. Both 90° phase shifting of the first nitrogen pulse for TPPI and incrementation in the t_2 evolution period were accomplished by a c-script macro executed on the Ω-500 spectrometer. 3D spectra were acquired as a series of ^1H–^1H 2D files with varying t_2 increments.

NOESY-HMQC and TOCSY-HMQC spectra contained 256 t_1 values for each fixed t_2 value. A total of 32 t_2 values were collected in both experiments to digitize the evolution of nitrogen signals. 1024 complex points were collected for the free induction decays along t_3. The NOESY-HMQC experiment was recorded with a mixing time of 100 ms. A total of 32 scans were acquired for each t_1 value. In the TOCSY-HMQC spectrum a MLEV-17 spin lock (Levitt & Freeman, 1981; Bax & Davis, 1985) was used with 35-μs delays (clean-TOCSY) to eliminate ROE effects (Griesinger et al., 1986). Four mixing times (37, 56, 74, and 93 ms) were coadded during acquisition; 16 transients (4 scans per mixing time) were collected for each t_1 value. The TOCSY-HMQC and NOESY-HMQC experiments required 64 and 128 h of acquisition time, respectively.

In order to remove artifacts from the residual H_2O line, the data were Fourier transformed with respect to t_3, prior to further Fourier transformations along the other dimensions; a dispersive baseline correction (Adler & Wagner, 1991) was applied on a Sun 3/260 workstation. The 32 2D files were then subsequently transformed in t_2 and t_3 by using the program FELIX (Hare Research) on a Silicon Graphics 4D/240 Iris computer. The 3D matrix was zero filled, resulting in a final frequency domain data set of 512 × 128 × 512 real points in ω_1, ω_2, and ω_3, respectively. The final storage size of the real matrix was ca. 134 megabytes, which was readily stored on a high-density 1/4 in. tape. The final digital resolution in ω_1 and ω_2 was, respectively, 14 and 12.5 Hz per point. Since only amide proton resonances are present after Fourier transformation of the acquisition time domain (t_3), the t_3 time domain was zero filled prior to transformation and then resized after transformation to eliminate the aliphatic half of the spectrum. This doubled the digital resolution along ω_3 to a final value of 8.14 Hz per point without a cumbersome increase in the data size.

Assignments were made using plots $\omega_1 \times \omega_3$ planes from both 3D matrices. The plots covered 5.2–11.5 and −2.5–11.6 ppm in ω_3 and ω_1, respectively. Each plot was 0.2 ppm/cm in each proton dimension. Slices were plotted with an in-house program on a HP RX plotter.

RESULTS

Sequential resonance assignment of oxidized flavodoxin was accomplished in two stages. The first phase consisted of spin system identification by ^1H 2D NMR. In this phase, spin system identification and limited sequential assignments were obtained by standard NMR methods on an unenriched sample of flavodoxin (Wüthrich, 1986). Three-dimensional ^{15}N–^1H NMR (Zuiderweg & Fesik, 1989; Marion et al., 1989) was then employed in the second phase to make the bulk of the sequential assignments. Using this approach, we were able to sequentially assign 165 of the 166 non-proline residues present in the protein.

Flavodoxin's size (>19 kDa) prohibits a detailed discussion of all sequential connectivities. We discuss in detail the sequential assignment of three stretches of residues. These stretches are as follows: (1) the C-terminal helix, (2) strand E of the β sheet, and (3) residues 56–63, which forms part of the FMN-binding site. Spectral features exhibited in the 3D spectra by each of these stretches will be presented along with the strategies used in their sequential assignment. Sequential assignment discontinuities will be addressed under Discussion. Spin system identification formed the basis for all sequential assignments, they will therefore be briefly discussed below.

Spin System Assignments. Flavodoxin contains 169 amino acids of which 3 are prolines. There are 28 negatively charged residues (16 aspartic and 11 glutamic acids), which account for the low isoelectric point (pH 3.79) of the protein. At the pH used in these studies (pH 6.6), flavodoxin carries a negative charge. This charge appears to inhibit aggregation, preventing resonance line broadening. This spectral feature resulted in excellent coherence transfer for those experiments relying on

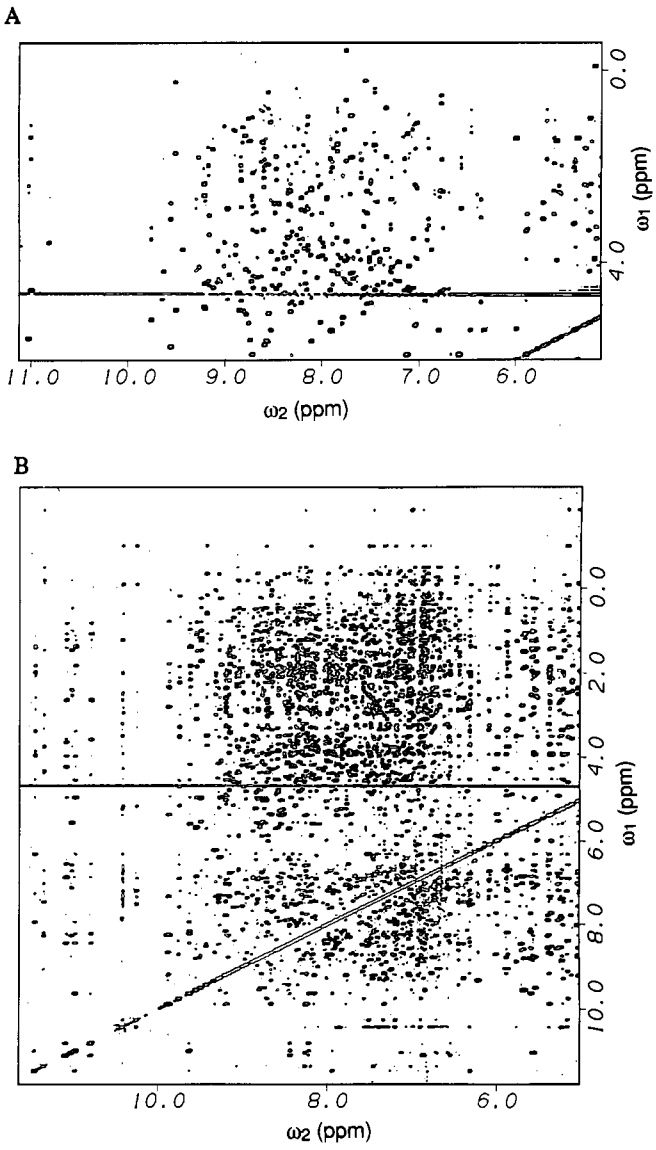

FIGURE 2: (A) ^1H TOCSY spectrum of oxidized flavodoxin in H_2O. The plot shows the downfield region that spans 11.1–5.5 ppm in ω_2 and 6.0 to −0.6 ppm in ω_1. A similar spectrum was used to identify and classify spin systems. Notice the efficient magnetization transfer out to the side chains. (B) ^1H NOESY spectrum of oxidized flavodoxin in H_2O. Severe resonance crowding inhibits spectral assignment. The plot shows the region spanning 4.9–11.5 ppm in ω_2 and 2.0–11.8 ppm in ω_1. A mixing time of 100 ms was used.

^1H–^1H scalar couplings for magnetization transfer (Figure 2A).

A series of 2D ^1H NMR experiments were performed on an unenriched sample of flavodoxin in H_2O. Figure 2A shows the region of a TOCSY spectrum collected in H_2O containing cross peaks between amide protons and aliphatic protons. This spectrum was used in conjunction with both DQF-COSY and DQ-COSY spectra to identify spin system networks. Emphasis was placed on correlating backbone amide proton resonances to their corresponding α protons. When possible, however, spin systems were classified into 9 categories: glycine, alanine, threonine, valine, leucine, isoleucine, long-chain, unknown, and AMX-type spin systems [where the term AMX classifies the symmetry of the aliphatic resonances (Wüthrich, 1986)].

Glycines were identified by observation of pairs of H^N-H^α cross peaks exhibiting large passive $^2J_{\alpha\alpha}$ couplings in the DQF-COSY and TOCSY spectra. Observation of remote cross peaks in a 2Q-COSY spectrum ($\omega_1 = C^\alpha H^1 + C^\alpha H^2$, $\omega_2 = H^N$) recorded in H_2O served to confirm the glycine assignments (Wagner & Zuiderweg, 1983). In this manner, we were able to unambiguously identify 14 of the expected 18 glycines present in flavodoxin prior to the sequential assignment stage. Alanines and threonines were identified in the TOCSY spectrum by the characteristic appearance of upfield-shifted β and γ methyl resonances, respectively. These two spin system types were differentiated through analysis of the aliphatic portion of the 2QF-COSY spectrum recorded in ^2H_2O. This analysis revealed whether the spin system and interest consisted of two resonances (alanine) or three (threonine). This analysis unambiguously identified eight alanine and seven threonine spin systems. Valine, leucine, or isoleucine spin systems were distinguished when possible by analysis of H_2O TOCSY and ^2H_2O 2QF-COSY and TOCSY spectra. Spin systems containing four spins and pairs of resonances between 2.5 and 3.9 ppm were classified as AMX-type systems. Long-chain systems were identified as multiple systems with resonances between 1.5 and 2.0 ppm. When only an H^N–H^α cross peak was present or the spin topology was ambiguous in both TOCSY or 2QF-COSY spectra, the spin system was placed in the unknown category.

Use of homonuclear data alone identified approximately 90% of the expected spin systems present in flavodoxin. Additional spin system assignments were made when the 3D TOCSY-HMQC data (Marion et al., 1989) became available. In general, however, homonuclear data laid the foundation for 3D data analysis.

Sequential Assignments. Figure 2B shows the downfield region of a NOESY spectrum recorded in H_2O on an unenriched sample of flavodoxin. The figure illustrates the crowding and resonance overlap present in the homonuclear NOESY spectrum of flavodoxin. Analysis of the homonuclear data yielded the sequential assignment of those residues with amide protons resolved from the bulk of amide and aromatic resonances. To facilitate the assignment of the majority of overlapped resonances, flavodoxin was uniformly enriched with ^{15}N. Figure 3 shows the 2D ^1H–^{15}N correlation spectrum of enriched oxidized flavodoxin in H_2O with all assigned resonances labeled according to sequence number as obtained after final assignments. This spectrum possesses several interesting features. In particular, the glycine amide nitrogens are distinguished from the bulk of the amide resonances by their upfield ^{15}N resonance position. This feature was subsequently exploited in the sequential assignment of these residues. Also shown in this spectrum are the characteristic downfield resonance positions of the $H^{\epsilon 1}$ and $^{15}N^{\epsilon 1}$ tryptophan nuclei. The ^1H–^{15}N correlation spectrum also allowed the assignment of the $^{15}N3$ and N3H resonances of the FMN ring (outside the spectral window), at 162.79 and 10.89, ppm, respectively; they are in good agreement with values reported for the homologous flavodoxin from *Anabaena* 7120 at pH 7.4 (Stockman et al., 1988).

We have acquired both 3D TOCSY-HMQC and NOESY-HMQC spectra in H_2O. These spectra were used to generate plots (32 cm × 75 cm) corresponding to every other (ω_1, ω_3) slice of the 3D matrix. Intraresidue information from the 3D TOCSY spectra was then transferred to the corresponding NOESY slice, analogous to the procedure used in homonuclear assignment methodology. Spin system information from the homonuclear analysis was then exploited to correlate known spin systems with their corresponding amide nitrogen resonances. A spin system table was constructed containing the ^1H resonance positions of all known spin systems and the ^{15}N chemical shift of the corresponding backbone amide. Sequential assignments were made by observation of

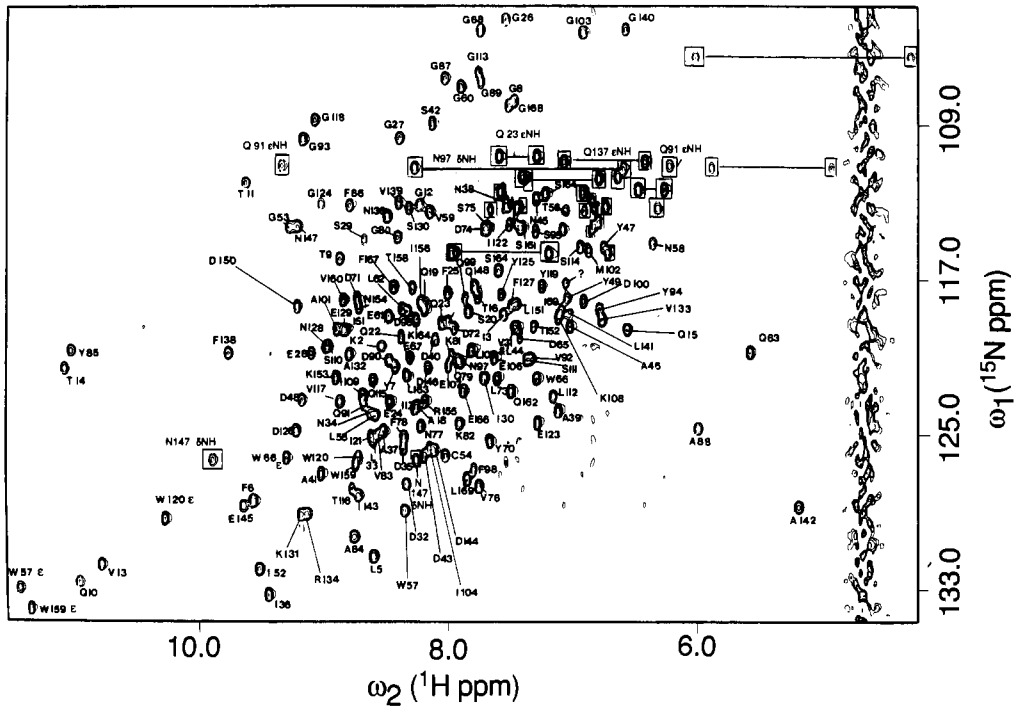

FIGURE 3: ^{1}H–^{15}N Correlation spectrum of uniformly enriched flavodoxin in H_2O. Assigned cross peaks are labeled according to the sequence number. Unassigned cross peaks are denoted by a "?". Lysine and arginine side-chain correlations are outside the spectral window of this figure. Unassigned side-chain ^{15}N–^{1}H correlations of asparagine and glutamine residues are boxed and unlabeled.

interresidue cross peaks in the NOESY spectrum followed by a search of all slices in the 3D TOCSY spectrum for the spin system giving rise to those cross peaks. This procedure was facilitated by referring to the chemical shift table. In this manner, spin systems were linked sequentially. Stretches of spin systems that were sufficiently unique were then readily placed into the sequence.

Assignment of Helical Regions

There are several short proton–proton distances that are characteristic of residues in helical conformations. Distances derived from polyalanine helices indicate that 2.8 and 4.2 Å separate amide protons that are adjacent (d_{NN}) and separated by one residue [$d_{NN}(i,i+2)$] in the sequence, respectively (Dubs et al., 1979; Billeter et al., 1982). We have exploited the short d_{NN} distance between adjacent residues to sequentially assign the majority of helical residues. The procedure used is as follows. A cross peak is identified as a d_{NN} NOE when the following three criteria are met: (1) It appears in the 3D NOESY-HMQC spectrum. (2) It is absent in the 3D TOCSY-HMQC spectrum. (3) There is a symmetrical cross peak about the diagonal in the 2D ω_2-edited NOESY spectrum (Otting et al., 1986; Bax & Weiss, 1987). Often the ω_2-edited NOESY spectrum shows a cross peak only on one side of the diagonal, indicating that the cross peak corresponds to an NOE between a proton attached to nitrogen-15 and a proton attached to another nucleus. When the above three criteria are met, the 3D NOESY-HMQC spectra is searched for the symmetrically related partner. It is important to note that the ^{15}N chemical shift position of the symmetrically related cross peak (i.e., ω_3–ω_1 slice) is readily determined by analysis of the 2D ^{1}H–^{15}N correlation spectrum.

Residues 150–169. Strong d_{NN} connectivities between these residues is indicative of helical secondary structure. Figure 4 illustrates the assignment of residues 158–169. This figure displays ω_1–ω_3 slices of the NOESY-HMQC spectrum. Each panel contains cross peaks for residues whose amide nitrogens resonate at the nitrogen-15 frequency of the slice (the ω_2 frequency is indicated at the top of each panel). Slices span 0.3 ppm on the ω_3 axis and contain cross peaks originating from the amide proton of the indicated residue (the residue name and amide proton chemical shift are given at the bottom of each panel). Residues L169–L164 (panels L–G) exhibit

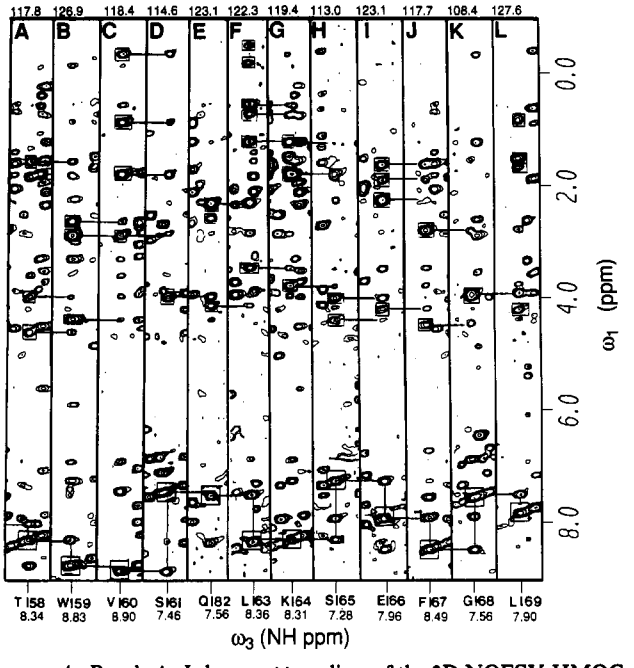

FIGURE 4: Panels A–J show $\omega_1 \times \omega_3$ slices of the 3D NOESY-HMQC spectrum. Slices are taken at the ω_2 axis position corresponding to the backbone amide nitrogen frequency of residues 169–158. Residue number and amide proton chemical shift are indicated below each slice. Amide nitrogen-15 chemical shifts are listed at the top of each panel. For clarity, each slice contains only 0.3 ppm of the ω_3 axis. Sequential d_{NN} cross peaks are connected with lines and appear downfield of 7.0 ppm on the ω_2 axis. Intraresidue amide-to-aliphatic proton cross peaks are boxed. Lines connect interresidue cross peaks to corresponding boxed intraresidue cross peaks of the preceding residue.

strong d_{NN} connectivities (connected cross peaks). The presence of $d_{N\alpha}(i,i-1)$ and $d_{N\beta}(i,i-1)$ connectivities between these residues lends support to their sequential assignment. The stretch of residues from 159 to 164, however, shows extensive amide proton chemical shift degeneracy, making their assignment from homonuclear data alone difficult. The amide protons of K164 and L163 are degenerate (panels F and G). This sequential assignment is based on connectivities at 3.83, 1.85, 0.81, and 0.62 ppm (panel G). The assignment is further substantiated by both $d_{N\alpha}(i,i-3)$ and $d_{N\alpha}(i,i-4)$ connectivities between NH of K164 and the $C^{\alpha}H$ protons of S161 and V160, respectively (not shown for clarity). A strong d_{NN} in addition to $d_{N\alpha}(i,i-1)$ and $d_{N\beta}(i,i-1)$ connectivities serves to link L163 and Q162 (panels F and E). The amide protons of Q162 and S161 are degenerate (panels D and E). The appearance of $d_{N\alpha}(i,i-1)$ and $d_{N\beta}(i,i-1)$ (panel E) led to this sequential assignment. Also present in panel E are several medium-range $d_{NN}(i,i+2)$ and $d_{NN}(i,i+3)$ NOE's to V160 and W159, respectively (not shown). The sequential assignment of S161 and V160 (panels D and C) shows all expected sequential connectivities. Amide proton degeneracy, however, occurs between V160 and W159 (panels C and B). As shown in panel C, however, this assignment is substantiated by both $d_{N\alpha}(i,i-1)$ (4.46 ppm) and $d_{N\beta}(i,i-1)$ (2.71 and 2.96 ppm) connectivities. The sequential assignment of T158 and W159 is supported by all expected connectivities as shown in panels A and B.

The sequential assignment of residues 150–159 is comparable to that discussed above. Strong $d_{NN}(i,i-1)$, $d_{N\alpha}(i,i-1)$, and $d_{N\beta}(i,i-1)$ connectivities are exhibited by adjacent residues. However, residues R155 and I156 are an exception. The amide protons of these residues are degenerate, and only one $d_{N\beta}(i,i-1)$ connectivity is observed. The sequence preceding I156 (T152-K153-N154-R155) is unique in the flavodoxin sequence and exhibits strong sequential connectivities. Side-chain spin system analysis of these residues with DQF-COSY and TOCSY spectra recorded in ^2H_2O unambiguously confirm their placement in the sequence. In addition, residue I156 shows clear sequential connectivity to K157. The sequence-specific assignment of R155 to I156 is further substantiated by the observation of medium-range NOE's from neighboring residues shown in Figure 8. Medium-range NOE's indicate that residues 12–21, 40–46, 103–114, 145–148, and 152–169 adopt helical conformations in solution.

Assignment of β Sheet Residues

Residues 141–145. As in 2D spectral analysis, sequential assignment of sheet residues in 3D spectra differed from that of helical residues. The process relied heavily on the observation of $d_{N\alpha}(i,i-1)$ connectivities because the d_{NN} distance was generally too long to be observed in the 3D NOESY-HMQC spectrum. Figure 5 shows how the sequential assignment of residues 141–145 was accomplished. Each panel of Figure 5 is an ω_1–ω_3 slice through the 3D NOESY-HMQC spectrum. The slices are taken at the nitrogen-15 frequency of the backbone amide nitrogen of the indicated residue (shown at the bottom of the panel) and contain a 0.3 ppm region of the ω_3 axis. Panels A–E contain residues 141–145, respectively. Intraresidue cross peaks are boxed and long-range NOE's are labeled.

Figure 5E contains cross peaks arising from the amide proton of E145. A $d_{N\alpha}(i,i-1)$ cross peak from D144 at 5.66 ppm sequential links the two residues. Intraresidue cross peaks of N144 are shown boxed in figure 5D. The strong $d_{N\alpha}(i,i-1)$ cross peak from I143 at 4.33 ppm along with other sequential cross peaks are illustrated by lines drawn from panel C to panel D. Panel C is a slice taken at the backbone nitrogen-15

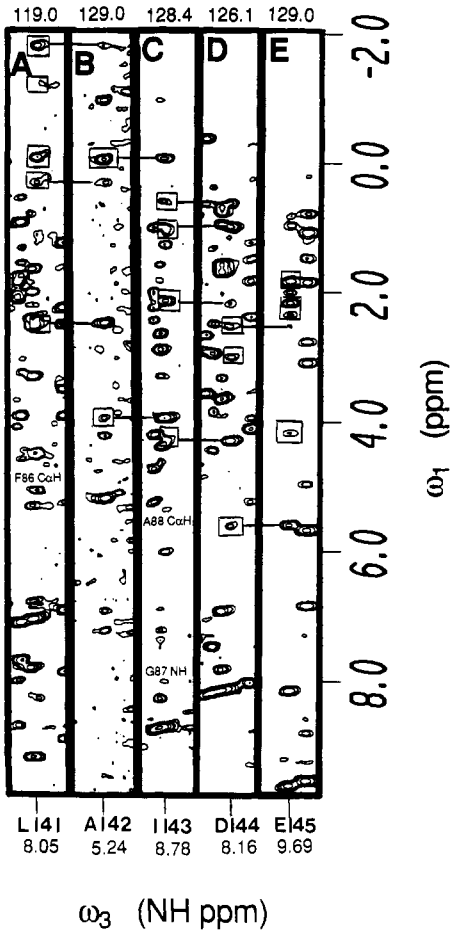

FIGURE 5: Panels A-E show $\omega_1 \times \omega_3$ slices of the 3D NOESY-HMQC spectrum. Slices are taken at the ω_2 axis position corresponding to the backbone amide nitrogen frequency of residues 141–145. The residue and its amide proton chemical shift are denoted at the bottom of each panel. The amide nitrogen-15 frequency of each residue is shown at the top of each panel. For clarity, each slice contains only 0.3 ppm of the ω_3 axis. Intraresidue cross peaks are boxed with lines drawn to the panel of the following residue to illustrate sequential connectivity. Some tertiary NOE's in panels A and C are labeled.

frequency of I143. Cross peaks at 5.24 and 0.0 ppm are interresidue $d_{N\alpha}(i,i-1)$ and $d_{N\beta}(i,i-1)$ connectivities to A142. In addition, the amide proton of I143 shows tertiary interstrand cross peaks. The cross peak at 5.42 ppm in panel 5C is an interstrand $d_{N\alpha}(i,j)$ connectivity to A88; a $d_{NN}(i,j)$ cross peak at 8.08 ppm to G87 is also observed. Panel B contains cross peaks arising from the amide proton of A142. The cross peak at 2.53 ppm is a cross peak to the $C^{\alpha}H$ proton of L141. The extreme upfield resonance position of the $C^{\alpha}H$ proton of L141 is consistent with ring current shift calculations conducted on the crystal structure of flavodoxin from *A. nidulans* (Brian Stockman, personal communication). Panel 5A contains the intraresidue cross peaks of L141. The boxed cross peaks at 4.5–4.6 ppm are $d_{N\alpha}(i,i-1)$ connectivities to G140. The cross peak at $\omega_1 = 5.11$ is an $d_{N\alpha}(i,j)$ interstrand connectivity to F86.

Sequence-specific assignment of all residues participating in the β sheet were obtained in a similar fashion. Tertiary NOE's illustrated in Figure 6 as arrows connecting residues allowed the topology of the sheet to be determined. The sheet consists of five strands that run in parallel. The overall topology is of the BACDE type where A–E represent amino acid stretches of increasing sequence number. This topology is in agreement with the crystal structure. Tertiary NOE's indicate that residues 3–9, 31–37, 49–56, and 81–89 form strands A–D, respectively. Strand E is comprised of two different sequential

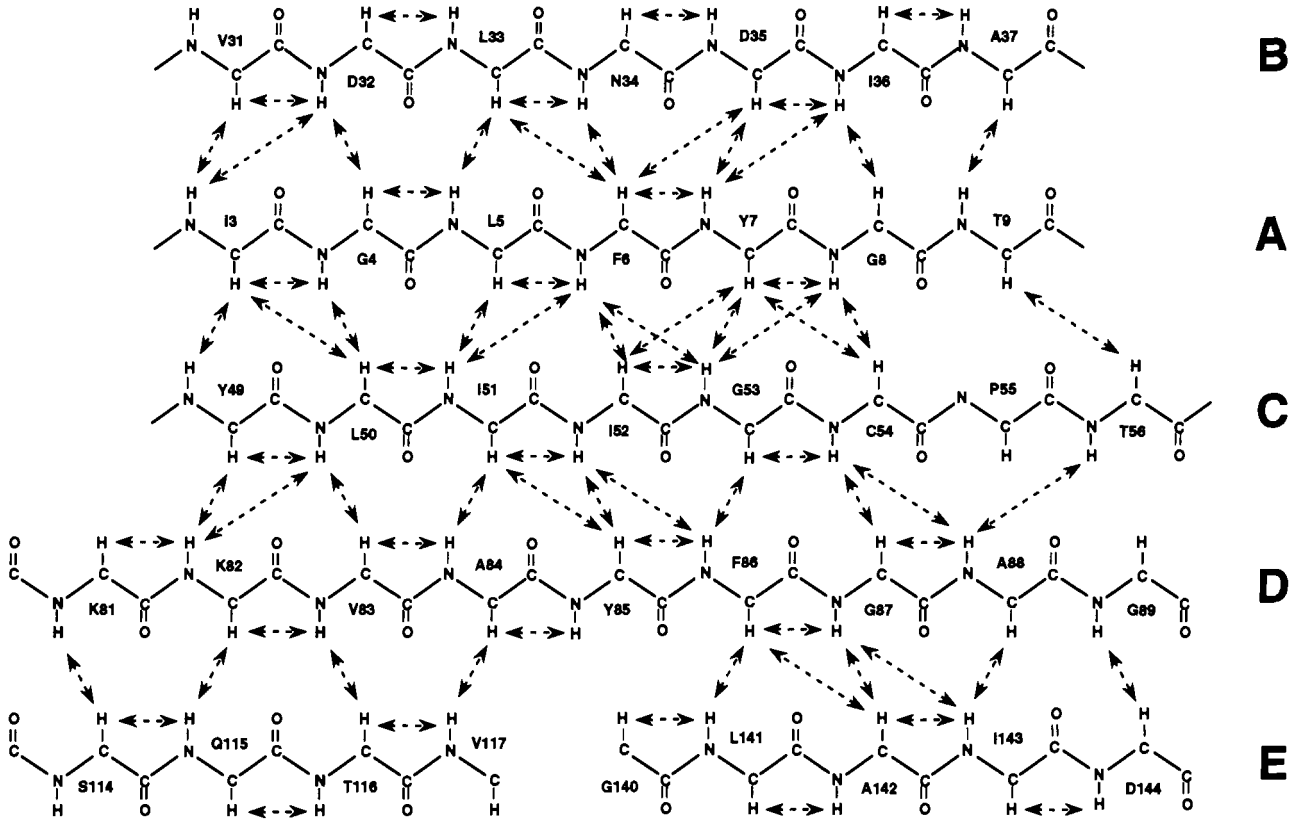

FIGURE 6: β Sheet topology of oxidized flavodoxin from *A. nidulans*. Arrows indicate observed tertiary NOE's. The β sheet is formed by residues 3–9, 31–37, 48–56, 81–89, 114–117, and 140–145. The majority of $d_{\alpha H-\alpha H}(i,j)$ NOE's were not observed due to spectral overlap.

stretches, residues 114–117 and 141–144. Apparent discrepancies with the crystal structure will be dealt with under Discussion.

FMN-Binding Site

Interpretation of protein–FMN interactions from NMR data depends on the validity of FMN resonance assignments and the assignment of protons attached to neighboring residues in the polypeptide. In the crystal structure of flavodoxin, residues 55–60 and 89–100 form part of the FMN-binding site (Ludwig et al., 1984). Therefore, presented below is an in-depth discussion of the sequential assignment of residues 56–62. The assignment of residues 89–100 is comparable to that of 56–60. Structural implications of observed FMN–protein NOE's will be presented under Discussion.

Residues 56–62. Figure 7 shows slices of the 3D NOESY-HMQC spectrum containing residues 56–62. Each slice contains cross peaks from those residues with amide ^{15}N chemical shifts denoted at the top of each panel. Intraresidue cross peaks are boxed. Residues E61 and L62 both appear in panel 7F. This phenomenon is readily explained by reference to Figure 3, which indicates that the amide ^{15}N chemical shifts of E61 and L62 are 119.2 and 118.9 ppm, respectively. Since the ω_2 digital resolution in the 3D spectra is 12.5 Hz per point, cross peaks from both residues are expected to appear in the same $\omega_1 \times \omega_3$ slice. The sequential assignment of E61 to L62 is based on both $d_{N\alpha}(i,i-1)$ and $d_{N\beta}(i,i-1)$ connectivities, no d_{NN} connectivity is observed. Panels 7D–F contain residues 59–61, respectively. Strong d_{NN} cross peaks are observed between these residues (connected resonances downfield) of ω_1 = 6.0 ppm). These residues are also tied by $d_{N\alpha}(i,i-1)$ and $d_{N\beta}(i,i-1)$ connectivities (upfield of ω_1 = 6.0 ppm). Panel 7C contains resonances of N58; the $d_{N\alpha}(i,i-1)$ (2.86 ppm) and $d_{N\beta}(i,i-1)$ (2.06 ppm) cross peaks of W57 are connected with lines to panel B. A faint d_{NN} cross peak also connects W57 to N58. Panel 7B contains W57 with all sequential connectivities to T56 apparent. The stretch of residues from 56 to 62 is unique in the sequence of flavodoxin, allowing unambiguous assignment.

Flavin ^1H and ^{15}N Resonance Assignments. Table I lists all assigned FMN nuclei. ^{15}N assignments of bound FMN in flavodoxins from other species have been reported previously (Vervoort et al., 1986; Stockman, 1989). These studies indicate that oxidized FMN ^{15}N resonances are positioned downfield of all polypeptide ^{15}N nuclei. Nitrogen-15 direct detection of oxidized flavodoxin from *A. nidulans* resulted in the observation of all expected downfield resonances. FMN nitrogen-15 assignments are based on chemical shift similarities with other flavodoxins and free FMN. The N3 atom of the isoalloxazine ring, however, was assigned unambiguously from its anomalous nitrogen-15 chemical shift in the 2D ^1H–^{15}N correlation spectrum of the protein. The attached proton (N3H) also exhibits NOE's in the NOESY spectra that are consistent with the crystal structure of the protein. Assignment of the C6H, C3H(7α), and C3H(8α) protons is based on NOE's to polypeptide protons that are consistent with the crystal structure. A ^{13}C–^1H heterocorrelation spectrum of unenriched flavodoxin in ^2H_2O (spectra not shown) substantiates the C3H(7α) and C3H(8α) assignments. In this spectrum, both C3H(7α) and C3H(8α) exhibit sharp correlations indicative of methyl resonances.

Comparison of bound FMN ^{15}N chemical shifts to those of free FMN in polar and tetraacetylriboflavin in nonpolar solvents facilitates an assessment of the extent of hydrogen bonding of a given isoalloxazine nitrogen-15 nucleus (Vervoort et al., 1986). Such a comparison has been made for the homologous flavodoxin from *Anabaena* 7120 (Stockman et al., 1988). The ^{15}N chemical shifts reported here are within ±0.7 ppm of the values reported for *Anabaena* 7120. The N5 chemical shifts of oxidized *A. nidulans* and *Anabaena* 7120

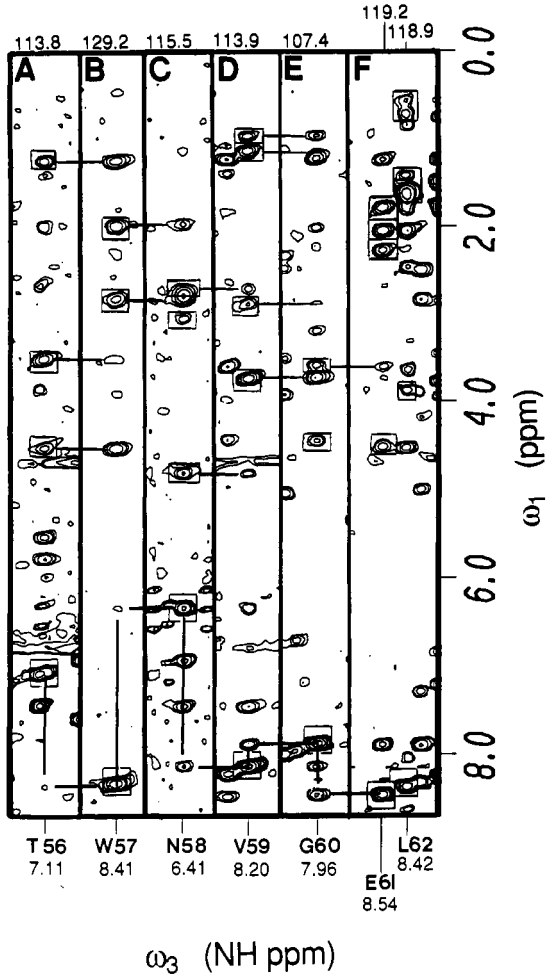

FIGURE 7: Panels A–F show $\omega_1 \times \omega_3$ slices of the 3D NOESY-HMQC spectrum. Slices are taken at the ω_2 axis position corresponding to the backbone amide nitrogen frequency of residues 56–62. The amide nitrogen-15 frequency of each residue is listed at the top of the panel. The amide proton chemical shift and residue name are denoted at the bottom of each panel. For clarity, each slice contains only 0.3 ppm of the ω_3 axis. Intraresidue cross peaks are boxed with lines drawn to the following residue to illustrate sequential connectivity. Sequential d_{NN} connectivities are joined by lines (downfield of ω_1 = 6.0 ppm).

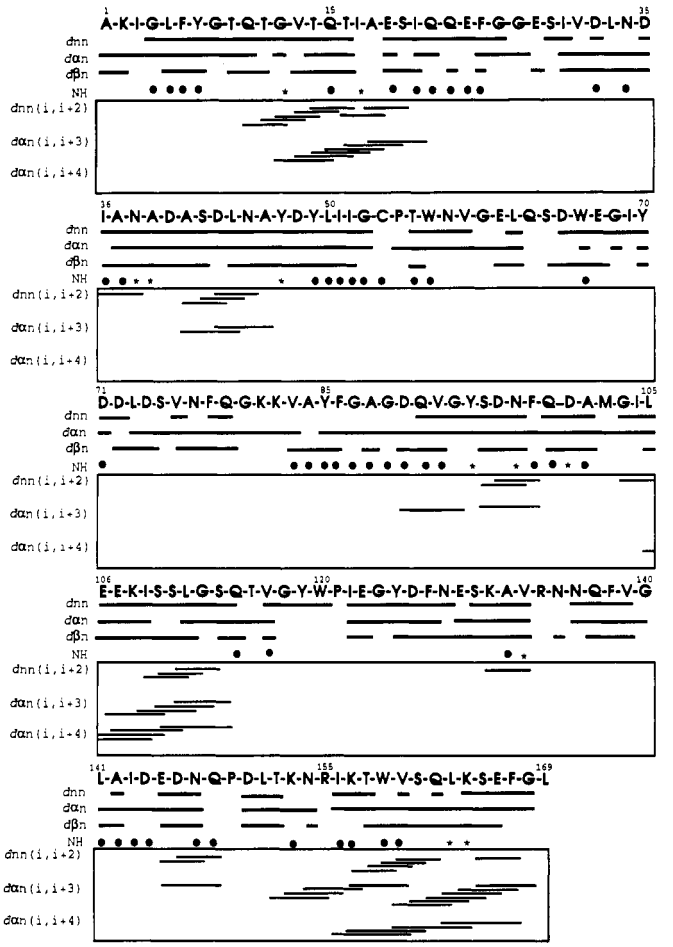

FIGURE 8: Summary of sequential and medium-range NOE's. The sequence is given with one-letter symbols for the amino acids. Lines 1–3 below the sequence give $(i,i+1)$ connectivities. In line 4, filled circles below the amino acids indicate residues with slowly exchanging amide protons. Asterisks below the amino acids indicate that the exchange rate of the amide proton is unknown because of resonance overlap. Medium-range NOE's typical of helical secondary structure are listed in lines 5–7.

flavodoxins indicate that the N5 atoms in both species are strongly hydrogen bonded to H_2O or to the polypeptide. The amide protons of N58 and V59 are potential hydrogen bond donors. The N3 and N1 atoms also form hydrogen bonds as judged by their downfield resonance positions compared to model compounds. In addition, the moderate proton exchange rate exhibited by the N3H proton when flavodoxin is dissolved in ^2H_2O indicates that it is at least partially shielded from solvent.

Discussion

We have assigned all backbone and a large fraction of side-chain resonances for 165 residues in flavodoxin. Excluding the three prolines in the protein, this leaves only S64 unassigned. Analysis of the ^1H–^{15}N correlation spectrum reveals a few unassigned H^N–^{15}N correlations that are candidates for the amide resonance of S64 or side-chain amine groups. These correlations are located in the spectral region dominated by side-chain amine resonances (11 asparagine and 11 glutamine residues) and do not exhibit transfer to aliphatic resonances in the 3D TOCSY-HMQC spectrum. Since S64 lies on the surface of the protein in the crystal structure, it may undergo rapid exchange with solvent, prohibiting assignment. Analysis of the DQF-COSY spectrum recorded in H_2O identified a faint NH–CαH correlation that may correspond to S64. The resonance position of this correlation is consistent with potential sequential NOE's [$d_{N\alpha}(i,i-1)$ and d_{NN}] exhibited by D65 in the 3D NOESY-HMQC spectrum. The assignment of S64 remains tentative.

The majority of sequence-specific assignments were based on several sequential connectivities as shown in Figure 8. However, a few residues were more challenging to assign. Resonance degeneracies and/or insufficient interresidue NOE's inhibited these assignments. The assignment of A1–K2 proved interesting. The $C^\alpha H$ and $C^\beta H$ protons of N-terminal alanines can readily be assigned from the HMBC spectra of a nitrogen-15 enriched protein (McIntosh et al., 1990; Oh et al., 1990). Utilizing this approach, we assigned these resonances for A1 along with its upfield-shifted N-terminal amine group (Table I). This assignment is substantiated by an intense $C^\alpha H$–$C^\beta H$ correlation in the 2QF-COSY spectrum and the absence of coherence transfer to a corresponding amide proton in the TOCSY spectrum recorded in H_2O. Weak resonances corresponding to K2 were assigned from a $d_{\alpha N}(i,i+1)$ cross peak to I3. In the 3D NOESY-HMQC spectra no observable NOE's to A1 were detected from the amide proton of K2. Analysis of the 2D homonuclear NOESY spectra, however, yielded faint $d_{N\alpha}(i,i-1)$ and $d_{N\beta}(i,i-1)$ cross peaks to A1 verifying the assignment.

Table I: Chemical Shifts for the Assigned Proton and Nitrogen Resonances of Oxidized Flavodoxin from *A. nidulans* at 30 °C, pH 6.6

residue	α-N	NH	H^{α}	H^{β}	others[a]
*A1	41.8		4.10	1.44	
*K2	120.7	8.61	4.31		1.96
I3	119.1	7.61	4.56		1.56, 0.31
G4	118.6	8.26	3.36, 1.61		
L5	131.6	8.65			1.92, 1.16, 1.11
F6	128.7	9.62	5.68	2.83, 3.16	
Y7	121.9	8.52	6.45	2.65, 2.93	
G8	118.6	7.53	4.89, 3.56		
T9	116.3	8.92	5.01	4.04	1.30 H^{γ}
Q10	132.9	10.98	4.61		1.90, 1.45, 1.19
T11	112.4	9.67	4.80		1.47 H^{γ}, 6.94 OH
G12	113.5	8.29	4.50, 3.67		
V13	132.0	10.79	3.65	2.64	1.14 H^{γ}, 0.90 H^{γ}
T14	121.9	11.10	3.71	4.31	1.31 H^{γ}
Q15	119.9	6.62	2.94		2.01, 2.11, 1.89
T16	118.2	7.81	4.41	4.01	1.31 H^{γ}
I17	124.0	8.32	3.49		1.99, 1.66, 1.26, 0.79, 0.46
*A18	123.8	8.31	3.56	1.31	
Q19	118.6	8.24	3.76		2.39, 2.16, 2.01
S20	119.0	7.90	4.31	4.11, 3.89	
I21	125.5	8.67	3.38		1.75, 1.54, 0.94, 0.56, −0.17
Q22	120.3	8.41	3.71		1.56
Q23	119.6	8.10	3.94		2.50, 2.24, 7.36 H^{ϵ}, 7.66 H^{ϵ}, 111.1 N^{ϵ}
E24	123.6	8.51	4.01		2.31, 2.06, 2.01
F25	118.0	8.06	3.91	3.03, 1.90	
G26	103.9	7.59	4.64, 3.74		
G27	110.1	8.44	4.66, 3.63		
E28	121.1	9.16	4.49		2.36, 216
S29	115.3	8.74	4.36	3.96	
I30	122.4	7.76	4.30		1.88, 1.01
V31	119.8	7.51	4.61		0.81, 0.53, 0.44
D32	127.8	8.41	4.91	2.41, 2.61	
L33	125.6	8.66	4.60	1.69, 1.53, 1.59	
N34	124.2	8.69	4.74	3.94, 1.95	
D35	126.1	8.42	3.55	2.64, 2.34	
I36	133.6	9.49	3.79		3.55, 0.66, −0.29
A37	125.1	8.57	3.83	1.14	
N38	113.6	7.59	4.90	3.03, 2.58	
A39	124.1	7.17	4.57	1.53	
D40	120.4	6.96	4.16	2.26, 2.56	
A41	127.3	9.06	3.65	1.14	
S42	109.3	8.16	3.86		
D43	126.4	8.25	4.51	3.01	
L44	119.8	7.52	3.86		1.63, 1.34, 0.81, 0.44, 0.37
N45	113.2	7.36	4.16	2.76	
A46	119.8	7.10	3.95	1.28	
Y47	115.7	6.81	4.61	3.35, 2.58	
D48	123.6	9.23	4.51	2.25, 2.04	
Y49	118.3	7.09	5.34	2.45, 1.69	
L50	124.3	8.61	5.66		2.06, 1.46
I51	119.9	8.87	5.04		1.55, 1.24
I52	132.3	9.56	5.03		1.79, 0.31
G53	114.7	9.33	4.14	1.87	
C54	126.4	8.08	5.27	2.43, 1.53	2.95 H^{S}
P55					
T56	113.8	7.11	4.56	3.56	1.28 H^{γ}
W57	129.2	8.41	2.86	2.06	6.38 δH, 11.47 ϵ^1H, 7.00 ϵ^3H, 8.00 ζ^2H, 7.08 ζ^3H, 7.33 η^2H, 133.2 εN
N58	115.5	6.41	4.87	3.13, 2.77	
V59	113.9	8.21	3.80	2.95	1.19 H^{γ}, 1.02 H^{γ}
G60	107.4	7.96	4.50, 3.67		
E61	119.2	8.54	4.61		2.35, 2.14, 1.86
L62	118.9	8.42	3.85		1.68, 1.63, 1.48, 0.77, 0.63
Q63	121.1	5.64	4.01		3.02, 2.89
*S64		8.45	3.98	3.76	
D65	120.1	7.49	4.51	2.81, 2.14	
W66	122.4	7.35	4.51	3.37, 3.27	7.45 δH, 9.35 ϵ^1H, 126.5 εN
E67	121.4	8.41	3.96		2.16, 2.26
G68	104.4	7.81	4.06, 3.86		
I69	118.9	7.15	4.63		1.79, 1.61, 1.36, 0.97, 0.57
Y70	125.7	7.73	4.01	3.41, 3.11	7.04 H^{δ}
D71	118.3	8.79	4.43	2.79, 2.69	
D72	119.9	8.02	4.78	2.76, 2.72	
L73	122.4	7.66	3.99		1.78, 1.31, 0.91, 0.74
D74	114.7	7.78	4.49	2.64	
S75	114.7	7.76	4.41		
V76	128.0	7.81	3.61	1.94	0.68 H^{γ}, −0.33 H^{γ}
N77	124.9	8.28	4.88	2.97, 2.72	

Table I (Continued)

residue	α-N	NH	H^{α}	H^{β}	others[a]
F78	125.4	8.41	4.22	3.19, 2.54	
Q79	121.6	8.02	3.96		2.56, 2.26, 2.16
G80	115.2	8.46	4.27, 3.84		
K81	121.3	7.98	4.61		1.91, 1.61, 1.46
K82	124.8	7.98	5.46		2.21, 1.96, 0.51
V83	125.3	8.61	5.09	2.03	0.87 H^{γ}, 0.53 H
A84	130.5	8.80	5.64	1.53	
Y85	121.0	11.08	5.60	2.60, 2.47	
F86	113.5	8.84	5.11	2.55, 2.39	
G87	107.0	8.08	4.00, 3.59		
A88	125.0	6.05	5.42	1.47	
G89	107.1	7.80	5.41, 3.98		
*D90	121.5	8.41	4.91	2.61, 2.41	
Q91	123.8	8.79	3.42		6.29 H^{ϵ}, 9.40 H^{ϵ}, 111.5 N^{ϵ}
V92	121.4	7.40	3.79		1.86, 0.84 H^{γ}
G93	110.1	9.23	3.48, 3.09		
Y94	118.9	6.83	4.61	2.71, 2.57	
S95	114.8	7.36	4.26	3.96	
D96	119.0	8.39	5.06	2.90, 2.58	
N97	121.6	7.96	5.45	3.27, 2.11	6.66 H^{δ}, 8.34 H^{δ}, 111.6 N^{δ}
F98	127.1	7.85	5.31	3.40, 2.69	
Q99	118.2	7.94	3.54	1.34	
D100	118.4	6.96	4.16	2.56, 2.29	
A101	119.9	8.95	3.69	1.31	
M102	115.9	6.92	3.80	2.12, 1.95, 1.79	
G103	104.6	6.98	3.59, 3.38		
I104	126.0	8.20	3.69		1.72, 0.83, 0.71
L105	121.0	7.86	3.96	1.46, 0.96	1.61 H^{γ}, 0.61 H^{δ}, −0.24 H^{δ}
E106	121.4	7.68	3.82		1.57, 0.21
E107	121.8	8.05	3.73		2.31, 2.20, 2.01
K108	119.2	7.21	4.14		2.15, 1.91, 0.91
I109	123.3	8.74	3.01		2.14, 0.66, 0.24, −0.10
S110	120.8	9.02	4.30	3.92	
S111	121.5	7.41	4.47	4.20, 4.12	
L112	123.4	7.21	4.63		2.16, 1.91
G113	106.7	7.81	4.46, 3.90		
S114	115.7	7.00	4.84	3.92, 3.76	
Q115	122.5	8.66	4.76		2.51, 2.31, 2.11
T116	128.1	8.82	5.29	4.24	1.06
V117	123.6	8.22	4.67	2.11	0.96 H^{γ}, 0.56 H^{γ}
G118	109.1	9.13	4.69, 3.82		
Y119	117.7	7.31	4.42	2.95, 2.82	
W120	126.5	8.78	5.93	3.37, 3.06	7.26 δH, 10.32 ϵ^1H, 8.25 ϵ^3H, 7.58 ζ^2H, 7.27 ζ^3H, 7.40 η^2H, 129.6 εN
P121					
I122	114.5	7.63	4.59		2.06, 1.22, 0.72, 0.27
E123	124.7	7.36	4.26		2.31, 2.06, 1.96
G124	113.4	9.11	4.13, 3.63		
Y125	118.1	7.63	5.09	3.30, 2.99	
D126	125.1	9.27	4.97	2.67, 2.43	
F127	118.7	7.54	4.89	3.31, 2.94	
N128	120.8	9.04	4.79		
E129	119.9	8.90	4.83		2.36, 2.15, 2.05
S130	113.7	8.37	4.86	3.96, 3.42	5.94 OH
K131	129.4	9.24	4.43		2.04, 1.67, 1.54, 0.82
A132	121.2	8.81	4.19	1.41	
V133	119.4	6.83	4.65	1.92	0.76 H^{γ}, 0.5 H^{γ}
R134	129.4	9.19	4.57		1.69
N135	126.5	9.36	4.22	2.93, 2.74	
N136	114.1	8.54	4.21	3.04, 2.84	
Q137	116.9	7.65	4.77		2.30, 2.18, 1.92 6.49 H^{ϵ}, 7.14 H^{ϵ}, 111.3 N^{ϵ}
F138	121.1	9.82	5.22	3.58, 3.33	
V139	113.4	8.46	3.96		
G140	104.4	6.64	4.51, 4.61		
L141	119.0	7.08	2.53		0.34, −0.04, −0.92, −1.73
A142	129.0	5.24	3.99	0.00	
I143	128.4	8.78	4.33		2.19, 1.04
D144	126.1	8.16	5.66	3.06, 2.57	
E145	129.0	9.69	4.24		2.40, 2.23, 1.91, 1.47
D146	121.9	8.21	4.61	2.89, 2.59	
N147	114.5	9.26	5.01	2.86, 2.41	8.32 H^{δ}, 9.95 H^{δ}, 126.6 N^{δ}
Q148	117.8	7.84	5.17		2.53, 2.27, 1.89
P149					
D150	118.7	9.26	4.48	2.77, 2.69	
L151	118.6	8.39	4.89		
T152	119.8	7.38	4.32	3.56	1.15 H^{γ}
K153	122.4	8.96	3.89		1.82, 1.69, 1.55

Table I (Continued)

residue	α-N	NH	H^{α}	H^{β}	others[a]
N154	118.8	8.77	4.57	2.79, 2.69	
*R155	123.6	8.24	4.24		2.09, 1.61
*i156	118.5	8.28	3.36		1.85, 0.79, 0.63
K157	119.5	8.05	3.65		1.90, 1.71, 1.40
T158	117.8	8.34	4.03	4.66	1.63 H^{γ}
W159	126.9	8.83	4.46	2.96, 2.71	7.53 δH, 11.41 ϵ^1H, 6.95 ϵ^3H, 8.33 ζ^2H, 6.56 ζ^3H, 6.78 η^2H, 134.6 εN
V160	118.4	8.90	3.52	1.86	0.95 H^{γ}, −0.26 H^{γ}
S161	114.6	7.46	4.03	3.98	
Q162	123.1	7.56	4.18		2.64, 2.43, 2.36
L163	122.3	8.36	3.51		1.31, 0.81, 0.62, −0.40, −0.10
K164	119.4	8.31	3.83		1.85, 1.29
S165	113.0	7.28	3.83	1.84, 1.29	
E166	123.1	7.96	4.25		2.36, 2.26, 1.96, 1.71
F167	117.7	8.49	4.49	2.86, 2.83	
G168	108.4	7.56	4.06, 3.96		
L169	127.6	7.90	4.29		1.75, 1.59, 0.93, 0.83

FMN Assignments	
nitrogen	proton
N1, 187.60; N3, 162.79	N3H 10.89
N5, 335.23; N10, 164.20	
	C6H, 7.51; CH3(7α), 2.77; CH3(8α), 2.71

[a] Resonances in "others" column that are not labeled belong to the spin system, but the position in the side chain is not known. Residues marked with an asterisk are tentatively assigned.

Resonance overlap caused the assignment of residues 30–36 to be rather difficult. These residues comprise one edge of the β sheet (strand A in Figure 6). Residues 29–31 are solvent accessible as evidenced by the rapid exchange of their amides (Figure 8). The amide protons of D32 and N34 exchange slowly with solvent, while those of V31 and L33 appear to exchange rapidly. These exchange properties are consistent with the crystal structure (illustrated in Figure 6). This figure clearly demonstrates that the amide protons of V31 and L33 do not participate in the hydrogen-bonding network of the β sheet while those of D32 and N34 form hydrogen bonds with the carbonyl oxygens of I3 and L5, respectively. Rapid amide exchange of I30 indicates that it is solvent accessible and therefore not a participant in the β sheet.

The sequential assignment of residues A18 and D90 remains tentative. Residues surrounding A18 (I17 and Q19) have been assigned with a high level of confidence. Unfortunately, ^{15}N and NH resonances believed to correspond to A18 are partially degenerate with residues I17, S44, N77. Several medium-range NOE's (Figure 8) serve to confirm this assignment. Resonances believed to correspond to D90 show strong sequential cross peaks to G89 [both $d_{N\alpha}(i,i-1)$ cross peaks], and resonances from D90 show sequential connnectivities to Q91. However, D90 does not possess several medium-range NOE's predicted by the crystal structure. Either this assignment is incorrect or the solution structure may show local differences with the crystal structure.

The assignment of C54 is worth mentioning. There are sequential cross peaks to G53 [two $d_{N\alpha}(i,i-1)$'s and a $d_{NN}(i,i-1)$]. In addition, cross-strand tertiary NOE's are observed from the amide proton of this residue. The TOCSY spectrum in H_2O shows cross peaks from the $C^{\alpha}H$ at 5.27 ppm to the NH at 8.08 ppm, two $C^{\beta}H$ protons at 2.43 and 1.53 ppm, and an additional signal at 2.95 ppm. This cross peak is only present in H_2O and absent in ^2H_2O. Therefore, it can be assigned to the proton of the free thiol group.

Secondary Structure of Flavodoxin in Solution. The crystal structure of *A. nidulans* flavodoxin indicates that it is an α/β-type protein with a five-stranded parallel β sheet at its core (Smith et al., 1983). Medium- and long-range, NOE's reveal that in solution flavodoxin maintains a secondary structure similar to the crystal structure. For example, medium-range NOE's [$d_{\alpha N}(i,i-3)$, $d_{\alpha N}(i,i+4)$, and $d_{NN}(i,i+2)$] indicate that residues 12–21, 103–114, and 152–169 form helices in solution (Figure 8). Residues 145–148 and 40–46 also show medium-range NOE's indicative of helical secondary structure, but because of their short length, participation in turns cannot be ruled out. When dihedral angles and hydrogen-bond distances are used as criteria for helix formation, the crystal structure predicts that residues 13–23, 40–46, 63–69, 100–110, 145–148, and 151–166 form α helices. Distance geometry calculations will reveal whether or not these discrepancies are significant.

Table II: Observed Protein–Flavin Mononucleotide NOE's

flavin proton	protein proton(s)	flavin proton	protein proton(s)
3	T56 α, β, γ	6	N58 NH
	V59 α, NH		V59 NH
	G60 NH[a]		V59 NH
	Y94 β_1, β_2		
	N97 α, β_1, β_2, NH[a]	7	W57 ϵ^3H, ζ^3H
	F98 α, NH		N58 NH,[b] α
	Q99 α		V59 NH
	D100 NH	8	W57 ϵ^3H, ζ^3H
6	N58 NH		

[a] The amide protons of G60 and N96 are degenerate. [b] N58 C^{β}H and C3H(7α) are degenerate.

Residues 3–9, 32–35, 49–56, 81–88, 115–117, and 141–143 participate in the β sheet in the crystal structure, while long-range NOE's indicate that residues 3–9, 31–37, 49–56, 81–89, 114–117, and 141–144 form the sheet. Figure 6 illustrates that the placement of residues V31, S114, and D144 into the β sheet is based on long-range NOE's to residues I3, K81, and G89, respectively. Close inspection of the crystal structure indicates that these NOE's are consistent with the crystal structure. The discrepancies can therefore be attributed to the different criteria used to define sheet participation.

FMN-Binding Site. The sequential resonance assignment of flavodoxin has yielded information about the FMN-binding site. Table II lists observed NOE's between the FMN and the apoprotein. The majority of these NOE's arise from the N3H proton. The assignment of this proton has already been discussed. Almost all cross peaks expected in the NOESY spectra between the N3H proton and the apoprotein are ob-

served (protons within 5 Å in the crystal structure). We do not, however, see an NOE between the $C^{\alpha}H$ protons of G60 and N3H, as would be expected from the crystal structure (these distances are 4.1 and 5.5 Å in the crystal structure). The confidence of the G60 assignment is quite high. Absence of the expected NOE may be a consequence of structural differences between the crystal and solution structures. Absence of NOE cross peaks from the N3H atom and the $C^{\alpha}H$ proton of Y94 and NH proton of Q99 indicates that the conformations of the FMN-binding site in *Anabaena* 7120 and *A. nidulans* are not identical [compare Stockman et al. (1990)].

There is substantial resonance overlap between other FMN protons and those of the protein. Enrichment with nitrogen-15 does not aid in their assignment since only one FMN proton is attached to nitrogen in the oxidized state. We were, however, able to assign the C6H, C3H(7α), and C3H(8α) protons from the ^{1}H NOESY spectra. These resonances show cross peaks to assigned residues consistent with the crystal structure. Resonance overlap, however, prevents complete characterization of NOE's arising from these protons. Unambiguous assignment of other FMN resonances will be obtained with ^{13}C enrichment of the FMN and/or the holoprotein.

We have been able to sequentially assign the majority of residues in flavodoxin. Analysis of the NOESY spectra indicates a wealth of structural information available from NOE identification and quantitative analysis. We have observed several long-range NOE's (Figure 6) that serve to define the overall global fold. Resonance assignment has yielded access to homo- and heteronuclear coupling constant information that will aid in defining backbone and side-chain conformations in solution. Backbone ^{15}N assignments facilitate the measurement of amide exchange rates and relaxation times. Measurements that yield dynamical information are not accessible from the crystal structure.

The primary goal of this research effort is to identify polypeptide–FMN interactions that modulate the reduction–oxidation potential of the bound FMN. Complete structural analysis of the FMN-binding site requires a wealth of NOE constraints not only from those protons attached to ^{15}N. Severe resonance crowding of the aliphatic region prohibits NOE cross peak analysis of carbon-attached protons. ^{13}C enrichment is therefore necessary to resolve these ambiguities.

Acknowledgments

We are indebted to Dr. Rowena Matthews for the generous use of her laboratory. We thank Drs. N. R. Nirmala and Brian Stockman for useful discussions. We express our appreciation to Dr. Martha Ludwig and Catherine Luschinsky for careful reading of the manuscript. The pKK233-2 vector carrying flavodoxin was generously provided by Dr. Neil A. Strauss, Department of Botany, University of Toronto. The *E. coli* strain W1485 was a gift from Dr. Barry Shane, Department of Nutritional Sciences, University of California at Berkeley. We thank Dr. D. Hare for providing FTNMR.

Registry No. FMN, 146-17-8.

References

Adler, M., & Wagner, G. (1991) *J. Magn. Reson. 91*, 450–454.

Bax, A., & Davis, D. G. (1985) *J. Magn. Reson. 65*, 355–360.

Bax, A., & Summers, M. F. (1986) *J. Am. Chem. Soc. 108*, 2093–2094.

Bax, A., & Weiss, M. A. (1987) *J. Magn. Reson. 71*, 571–575.

Bax, A., Freeman, R., Frenkiel, T. A., & Levitt, M. H. (1981) *J. Magn. Reson. 43*, 478–483.

Billeter, M., Braun, W., & Wüthrich, K. (1982) *J. Mol. Biol. 155*, 320–346.

Bodenhausen, G., & Ruben, D. L. (1980) *Chem. Phys. Lett. 69*, 185–188.

Braunschweiler, L., & Ernst, R. R. (1893) *J. Magn. Reson. 53*, 521–528.

Brown, S. C., Weber, P. L., & Mueller, L. (1988) *J. Magn. Reson. 77*, 166–169.

Burnett, R. M., Darling, G. D., Kendall, D. S., LeQuesne, M. E., Mayhew, S. G., Smith, W. W., & Ludwig, M. L. (1974) *J. Biol. Chem. 249*, 4383–4392.

Draper, R. D., & Ingraham, L. L. (1968) *Arch. Biochem. Biophys. 125*, 802–808.

Dubs, A., Wagner, G., & Wüthrich, K. (1979) *Biochim. Biophys. Acta 577*, 177–194.

Entsch, B., & Smillie, R. M. (1972) *Arch. Biochem. Biophys. 151*, 378–386.

Fukuyama, K., Wakabayashi, S., Matsubara, H., & Rogers, L. J. (1990) *J. Biol. Chem. 265*, 15804–15812.

Griesinger, C., Otting, G., Wüthrich, K., & Ernst, R. R. (1988) *J. Am. Chem. Soc. 110*, 7870–7872.

Hershey, A. D. (1955) *Virology, 1*, 108–127.

Jeener, J., Meier, B. H., Bachmann, P., & Ernst, R. R. (1979) *J. Chem. Phys. 71*, 4546–4553.

Kumar, R. M., Ernst, R. R., & Wüthrich, K. (1980) *Biochem. Biophys. Res. Commun. 95*, 1–6.

Laudenbach, D. E., Reith, M. E., & Straus, N. A. (1988) *J. Bacteriol. 170*, 258–265.

Levitt, M. H., & Freeman, R. (1981) *J. Magn. Reson. 43*, 65–80.

Levy, G. C., & Lichter, R. L. (1979) *Nitrogen-15 Nuclear Magnetic Resonance Spectroscopy*, John Wiley & Sons, New York.

Ludwig, M. L., Pattridge, K. A., & Tarr, G. (1984) in *Flavins and Flavoproteins* (Bray, R. C., Engel, P. C., & Mayhew, S. D., Eds.) p 253, deGruyter, New York.

Luschinsky, C. L., Dunham, W. R., Osborne, C., Pattridge, K. A., & Ludwig, M. L. (1991) in *Flavins and Flavoproteins* (Curti, B., Zuneth, G., & Ronchi, S., Eds.), de Gruyter, New York.

McIntosh, L. P., Wand, A. J., Lowry, D. F., Redfield, A. G., & Dahlquist, F. W. (1990) *Biochemistry 29*, 6341–6362.

Marion, D., & Wüthrich, K. (1983) *Biochem. Biophys. Res. Commun. 113*, 967–974.

Marion, D., Driscoll, P. C., Kay, L. E., Wingfield, P. T., Bax, A., Gronenborn, A., & Clore, G. M. (1989) *Biochemistry 28*, 6150–6156.

Mayhew, S. G., & Massey, V. (1969) *J. Biol. Chem. 244*, 794–802.

Mayhew, S. G., & Ludwig, M. L. (1975) *Enzymes (3rd ed.) 12*, 57–118.

Mierlo van, C. P. M., Vervoort, J., Muller, F., & Bacher, A. (1990a) *Eur. J. Biochem. 187*, 521–541.

Mierlo van, C. P. M., Lijnzaad, P., Vervoort, J., Muller, F., Berendsen, H. J. C., & Vlieg de, J. (1990b) *Eur. J. Biochem. 194*, 185–198.

Mierlo van, C. P. M., Sanden van der, B. P. J., Woensel van, P., Muller, F., & Vervoort, J. (1990c) *Eur. J. Biochem. 194*, 199–216.

Morris, G. A., & Freeman, R. (1979) *J. Am. Chem. Soc. 101*, 760–762.

Oh, B., Mooberry, E. S., & Markley, J. L. (1990) *Biochemistry 29*, 4004–4011.

Otting, G., Senn, H., Wagner, G., & Wüthrich, K. (1986) *J. Magn. Reson. 70*, 500–505.
Piantini, U., Sørensen, O. W., & Ernst, R. R. (1982) *J. Am. Chem. Soc. 104*, 6800–6801.
Rance, M., Sørensen, O. W., Bodenhausen, G., Wagner, G., Ernst, R. R., & Wüthrich, K. (1983) *Biochem. Biophys. Res. Commun. 117*, 479–485.
Shaka, A. J., & Freeman, R. (1983) *J. Magn. Reson. 51*, 169–173.
Shaka, A. J., Keeler, J., Frenkiel, T., & Freeman, R. (1983) *J. Magn. Reson. 52*, 335–338.
Smillie, R. M. (1965) *Biochem. Biophys. Res. Commun. 20*, 621–629.
Smith, W. W., & Ludwig, M. L. (1974) *J. Biol. Chem. 249*, 4383–4392.
Smith, W. W., Burnett, R. M., Darling, G. D., & Ludwig, M. L. (1977) *J. Mol. Biol. 117*, 195–225.
Smith, W. W., Pattridge, K. A., Ludwig, M. L., Petsko, G. A., Tsernoglou, D., Tanaka, M., & Yasunobu, K. T. (1983) *J. Mol. Biol. 165*, 737–755.
Stockman, B. J., Westler, W. M., Mooberry, E. S., & Markley, J. L. (1988) *Biochemistry 27*, 136–142.
Stockman, B. J., Reily, M. D., Westler, W. M., Ulrich, E. L., & Markley, J. M. (1989) *Biochemistry 28*, 230–236.
Stockman, B. J., Krezel, A. M., Markley, J. L., Leonhardt, K. G., & Straus, N. A. (1990) *Biochemistry 29*, 9600–9609.
Tollin, G., & Edmondson, D. E. (1980) *Methods Enzymol. 69*, 392–406.
Vervoort, J., Muller, F., Mayhew, S. G., van den Berg, W. A. M., Moonen, C. T. W., & Bacher, A. (1986) *Biochemistry 25*, 6789–6799.
Wagner, G., & Zuiderweg, E. R. P. (1983) *Biochem. Biophys. Res. Commun. 113*, 854–860.
Watenpaugh, K. D., Sieker, L. C., & Jensen, L. M. (1973) *Proc. Natl. Acad. Sci. U.S.A. 70*, 3857–3860.
Watt, W., Tulinsky, A., Swenson, R. P., & Watenpaugh, K. D. (1991) *J. Mol. Biol.* (in press).
Wüthrich, K. (1986) *NMR of Proteins and Nucleic Acids*, Wiley, New York.
Wüthrich, K., Billiter, M., & Braun, W. (1984) *J. Mol. Biol. 180*, 715–740.
Zuiderweg, E. R. P., & Fesik, S. W. (1989) *Biochemistry 28*, 2387–2391.

Two- and Three-Dimensional Proton NMR Studies of Apo-Neocarzinostatin

Xiaolian Gao* and William Burkhart

Structural and Biophysical Chemistry, Glaxo Research Institute, 5 Moore Drive, Research Triangle Park, North Carolina 27709

Received February 26, 1991; Revised Manuscript Received April 25, 1991

ABSTRACT: Neocarzinostatin (NCS) is an antitumor protein from *Streptomyces carzinostaticus* that is identical in apo-protein sequence with mitomalcin (MMC) from *Streptomyces malayensis*. We describe the use of apo-NCS as a model system for applying combined two- and three-dimensional (2D and 3D) proton NMR spectroscopy to the structure determination of proteins (M_r > 10K) without isotope labeling. Strategies aimed at accurately assigning overlapped 2D cross-peaks by using semiautomated combined 2D and 3D data analysis are developed. Using this approach, we have assigned 99% of the protons, including those of the side chains, and identified about 1270 intra- and interresidue proton–proton interactions (fixed distances are not included) in apo-NCS. Comparing our results with those reported recently on 2D NMR studies of apo-NCS [Adjadj, É., Mispelter, J., Quiniou, É., Dimicoli, J.-L., Favadon, V., & Lhoste, J.-M. (1990) *Eur. J. Biochem. 190*, 263–271; Remerowski M. L., Glaser, S. J., Sieker, L., Samy, T. S. A., & Drobny, G. P. (1990) *Biochemistry 29*, 8401–8409] demonstrated advantages of proton 3D NMR spectroscopy in protein spectral assignments. We are able to obtain more complete proton resonance and secondary structural assignments and find several misassignments in the earlier report. Strategies utilized in this work should be useful for developing automation procedures for spectral assignments.

Several considerations have contributed to the initiation of the studies of antitumor proteins mitomalcin (MMC) and neocarzinostatin (NCS) isolated from various species of *Streptomyces* (Ishida et al., 1965; McBride et al., 1965). Actinoxanthin and auromomycin are the other two members known to this antitumor protein family (Montgomery et al., 1981). MMC, NCS, and auromomycin are structurally interesting. Each of these proteins is believed to contain a nonprotein component noncovalently bound to the apoprotein, which presumably protects the labile nonprotein molecule from decomposition in aqueous solution (Napier et al., 1979; Suzuki et al., 1980; Montgomery et al., 1981; Naoi et al., 1982). These ligand–protein complexes are important models for understanding fundamental aspects of specific molecular recognition between ligands and protein host molecules. The nonprotein component in NCS has been well characterized in solution (Goldberg, 1986; Myers et al., 1988). It contains a highly active diynene cyclic moiety and was shown to cause chain cleavage along the DNA backbone (Lee & Goldberg, 1989; Jung & Kohnlein, 1981). However, information about the identities and structures of the nonprotein components in apoproteins other than NCS and the mechanisms of the in vivo antitumor activities are still lacking. Progress in this area is awaiting high-resolution structural information for both apo- and holoproteins. High-resolution crystal structures of actinoxanthin and apo-auromomycin have been reported (Pletnev

0006-2960/91/0430-7730$02.50/0